Available online at www.eccomasproceedia.org
Eccomas Proceedia COMPDYN (2025) 6205-6216

ECCOMAS
Proceedia

COMPDYN 2025
10th ECCOMAS Thematic Conference on
Computational Methods in Structural Dynamics and Earthquake Engineering
M. Papadrakakis, M. Fragiadakis (eds.)
Rhodes Island, Greece, 15-18 June 2025

ANALYTICAL STUDY ON CYCIC LOCAL BUCKLING BEHAVIOR AND SEISMIC PERFORMANCE OF JOINT PANELS OF SQUARE STEEL TUBE COLUMNS AND H-SHAPED STEEL BEAMS

Kohei Tanaka[1] and Kosuke Sato[2]

[1] Graduate Student, Department of Architecture, Graduate School of Engineering, Mie University
e-mail: 424M415@m.mie-u.ac.jp

[2] Associate Professor, Department of Architecture, Graduate School of Engineering, Mie University, Doctor of Engineering
e-mail: sato@arch.mie-u.ac.jp

Abstract

In Japan, square steel tube columns and H-shaped steel beams are commonly used in steel buildings. The joint panels of the beam-column connections are the members which receive bending from both the columns and beams. Since the joint panels have the short length, the panel is strongly affected by shear. Due to the effect of shear, it is known that the local buckling may occur on the panel webs. Since the elasto-plastic deformation of the joint panels significantly affects the large deformation behavior of the overall frame, the relationship between the local buckling behavior and plastic deformation capacity of joint panels provides important insights.

Many previous studies on the local buckling and the plastic deformation capacity of panels have been investigated. However, the relationship between the local buckling strength and the plastic deformation capacity of the panels is not sufficiently investigated by analysis.

The purpose of this study is to investigate the elastic local buckling strength and plastic deformation capacity of the joint panels with the energy method analysis and finite element method analysis. In addition, seismic performance is reasonably evaluated based on the buckling strength.

In the present paper, the effect of the loading condition on the joint panels on the elastic local buckling strength is considered. In addition, the local buckling strength is evaluated quantitatively with buckling coefficient. Regarding seismic performance of the joint panels, the ultimate strength and plastic deformation capacity are reasonably evaluated with the normalized width–thickness ratio.

Keywords: Steel structure, Square hollow section member, Shear buckling, Ultimate strength, Plastic deformation capacity, Width–thickness ratio

doi: 10.7712/120125.1288 .25871

1 INTRODUCTION

the steel moment-resisting frames can have high toughness, absorb seismic energy, and provide stable behavior during strong earthquakes. In addition, since the moment frames make large open spaces without walls, the moment frames are widely used in seismic-prone areas such as Japan. In Japan, square steel tube columns and H-shaped steel beams are commonly used in the structural type of steel buildings. Joint panels of the beam-column connection are members which transmit stresses between the columns and beams, and receive bending from both the beams and columns. Since the joint panels have the short length, the joint panels is significantly affected by shear. Due to the effect of shear, it is known that the local buckling may occur on panel webs. The buckling is a significant factor determining the seismic performance of the members. Since the elsto-plastic deformation of the joint panels has significant effects on the large deformation behavior of overall frame, the seismic performance with considering the local buckling behavior is important within the current designing field focused on energy absorption capacity.

Many previous studies on the local buckling strength and plastic deformation capacity of the joint panels have been conducted. Namba et al. conducted loading experiments and analyses on steel tube panels with cross-sectional shapes and manufacturing methods as parameters, demonstrating the validity of calculating the full plastic strength using the effective volume panel [1]. Ikarashi et al. derived the elastic shear buckling strength of joint panels in the L-shaped connection composed of H-shaped beam-column. The effect of the stress state in the beams and columns is small, and the elastic shear buckling strength is almost determined by the shape of joint panels in the beam-column connection [2]. Kuwahara et al. conducted the shear loading experiments on the steel tube panels and highlighted the restraint effect of the H-shaped beam web attached to the panel flange, pointing out that it affects the buckling behavior [3]. Kumano et al. conducted the loading experiments on the square steel tube column and H-shaped steel beam connection frames. They confirmed that when the panel width–thickness ratio is large, the ultimate strength of the joint panels may be determined by shear buckling of the panel web [4]. Mou et al. performed repeated loading experiments on the stepped panels and confirmed that the ultimate strength is determined by the shear buckling occurring in the panel web [5]. Hwang et al. found that weld quality and panel zone design significantly influence the ductility and seismic performance of steel beam-to-column connections under cyclic loading [6]. Li et al. analyzed H-section connections showed where plastic damage begins and spreads, providing insights for better seismic design and code development [7].

In this context, many studies have been conducted on the seismic performance of the joint panels. However, the effects of loading conditions and member shapes on the elastic local buckling strength of the square hollow section joint panels are not sufficiently clarified. In addition, the seismic performance of the square steel tube joint panels is not sufficiently evaluated with considering the effects of loading conditions and member shapes.

The purpose of this study is to investigate the elastic local buckling strength of the joint panels with the energy method analysis and the elasto-plastic deformation behavior of the joint panels with finite element method analysis. In addition, the ultimate strength, plastic deformation capacity, and cumulative plastic deformation capacity as the seismic performance are reasonably evaluated considering the local buckling strength.

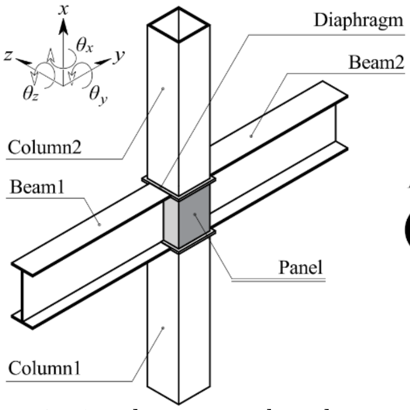

Fig. 1 Planar cross-shaped beam-column connection frame

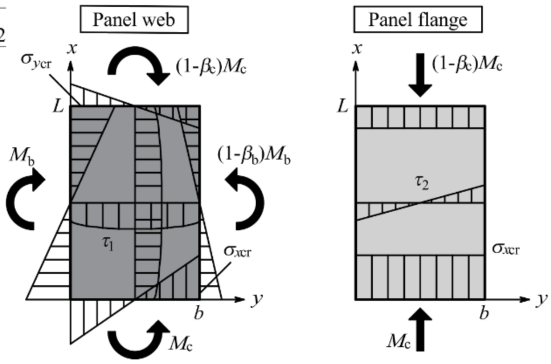

Fig. 2 Stress distribution

2 ELASTIC LOCAL BUCKLING ANALYSIS OF SQUARE HOLLOW SECTION JOINT PANELS

Fig. 1 shows the target of this analysis, the square hollow section joint panels of planar cross-shaped beam-column connection frame. In this chapter, the elastic local buckling strength of the panel webs and panel flanges which compose the joint panels is derived with the energy method [8]. Since the joint panels are much significantly affected by shear, the elastic local buckling strength of the joint panels is evaluated with shear buckling coefficient.

2.1 Overview of energy method analysis

The relationship between the elastic buckling stress and the shear buckling coefficient is given by Eq. (1). In this study, the shear buckling coefficient is used for the quantitative evaluation of the elastic local buckling strength.

$$\tau_{\rm cr} = \frac{\pi^2 E}{12(1-\nu^2)}\left(\frac{t}{b}\right)^2 \cdot k_\tau \tag{1}$$

Here, E is Young's modulus, ν is Poisson's ratio ($\nu = 0.3$), b is width of plate elements, and t is thickness of plate elements.

The strain energy and work done by external forces, as shown in Eqs. (2) and (3) respectively, are used to derive the buckling coefficient by solving the buckling condition equation (4) as eigenvalue problems.

$$\varDelta U_i = \frac{1}{2} D \int_0^L \int_0^b \left[\left(\frac{\partial^2 w_i}{\partial x^2} + \frac{\partial^2 w_i}{\partial y^2} \right)^2 - 2(1-\nu) \left\{ \frac{\partial^2 w_i}{\partial x^2} \frac{\partial^2 w_i}{\partial y^2} - \left(\frac{\partial^2 w_i}{\partial x \partial y} \right)^2 \right\} \right] dxdy \tag{2}$$

$$\Delta T_i = \frac{1}{2} t \int_0^L \int_0^b \left\{ \sigma_{xi}(x,y) \left(\frac{\partial w_i}{\partial x} \right)^2 + \sigma_{yi}(x,y) \left(\frac{\partial w_i}{\partial y} \right)^2 - 2\tau_i(x,y) \frac{\partial w_i}{\partial x} \frac{\partial w_i}{\partial y} \right\} dxdy \tag{3}$$

$$\frac{\partial \Delta U_i}{\partial a_{mn}} = \frac{\partial \Delta T_i}{\partial a_{mn}} \tag{4}$$

Here, i is number of plate elements. $i = 1$ indicates webs and $i = 2$ indicates flanges.

Fig. 2 shows the stress distribution in the plate elements. The panel webs receive the column bending moment $M_{\rm c}$ and the beam bending moment $M_{\rm b}$ in the two orthogonal directions. The relative sizes of bending moments are defined by the gradients of bending moment $\beta_{\rm c}$ and $\beta_{\rm b}$. Here, $\sigma_{x\rm cr}$ is maximum bending stress in the x-axis direction, and $\sigma_{y\rm cr}$ is maximum bending stress in the y-axis direction. L is length of plate elements, and b is width of plate elements. On the other hand, the panel flanges receive compression in the x-axis direction. Eqs. (5)–(9) are the stress functions based on the stress distribution in Fig. 2.

$$\sigma_{x1}(x,y) = -\sigma_{x\mathrm{cr}} \cdot \left(\frac{\beta_\mathrm{c} x}{L} - 1\right)\left(\frac{2y}{b} - 1\right) \tag{5}$$

$$\sigma_{y1}(x,y) = -\sigma_{y\mathrm{cr}} \cdot \left(\frac{\beta_\mathrm{b} y}{b} - 1\right)\left(\frac{2x}{L} - 1\right) \tag{6}$$

$$\tau_1(x,y) = \frac{1}{bL}\left\{\sigma_{x\mathrm{cr}} \cdot \beta_\mathrm{c}\left(-y^2 + by + \frac{1}{2}b^2\right) + \sigma_{y\mathrm{cr}} \cdot \beta_\mathrm{b}(-2x^2 + 2Lx)\right\} \tag{7}$$

$$\sigma_{x2}(x) = -\sigma_{x\mathrm{cr}} \cdot \left(\frac{\beta_\mathrm{c} x}{L} - 1\right) \tag{8}$$

$$\tau_2(y) = \sigma_{x\mathrm{cr}} \cdot \frac{\beta_\mathrm{c}}{bL}\left(-by + \frac{1}{2}b^2\right) \tag{9}$$

Furthermore, the displacement functions w_i are shown in Eqs. (10) and (11). The displacement function μ_m in the x-axis direction is shown in Eq. (12) and the displacement functions ${}_\mathrm{w}\nu_n$ and ${}_\mathrm{f}\nu_n$ in the y-axis direction are shown in Eqs. (13) and (14). In these functions, the deformation of plate elements is expressed with trigonometric functions. Here, ${}_\mathrm{w}\nu_n$ is the displacement function for the y-axis direction of the panel webs, and ${}_\mathrm{f}\nu_n$ is the displacement function for the y-axis direction of the panel flanges. The restraint effect of H-shaped section beam webs is considered in ${}_\mathrm{f}\nu_n$.

$$w_1 = \sum_{m=1}^{M}\sum_{n=1}^{N} a_{mn}\mu_m {}_\mathrm{w}\nu_n \tag{10}$$

$$w_2 = \sum_{m=1}^{M}\sum_{n=1}^{N} a_{mn}\mu_m {}_\mathrm{f}\nu_n \tag{11}$$

$$\mu_m = \sin\frac{m\pi x}{L} \qquad \text{(Simply supported at both ends)} \tag{12}$$

$${}_\mathrm{w}\nu_n = \sin\frac{n\pi y}{b} \qquad \text{(Simply supported along longitudinal edges)} \tag{13}$$

$${}_\mathrm{f}\nu_n = \sin\frac{2n\pi y}{b} \qquad \begin{pmatrix}\text{Simply supported along longitudinal edges} \\ \text{Simply supported along centerline}\end{pmatrix} \tag{14}$$

Fig. 3 shows the convergence of solutions. The vertical axis of Fig. 3(a) represents the shear buckling coefficient k_τ, while the horizontal axis represents the wave number M in the x-axis

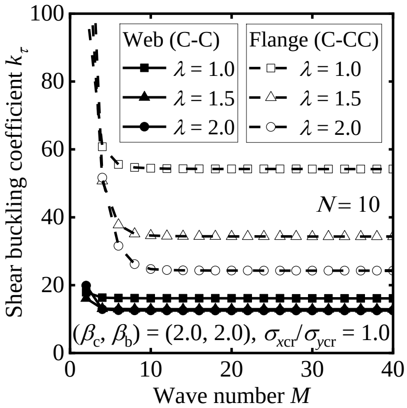

(a) Effect of M

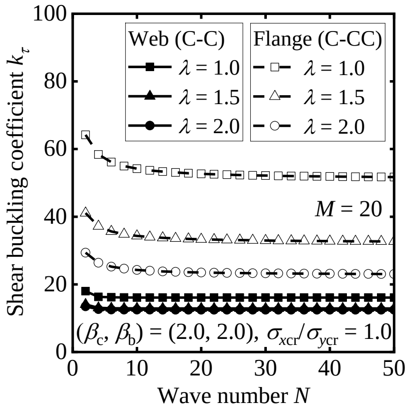

(b) Effect of N

Fig. 3 Convergence of solution (Clamped along 4 edges of plate element) direction. On the other hand, the horizontal axis of Fig. 3(b) represents the wave number N in the y-axis direction. The figures show the case where the solution converges most slowly, which is the 4 edges of the plate elements clamped support (C-C on panel webs and C-CC on panel flanges) case. In Figs. 3(a) and 3(b), it can be concluded that the solution converges sufficiently at around $M = 20$ and $N = 20$. Therefore, the wave numbers used in this study are $M = 20$ and $N = 20$ for both the panel webs and panel flanges.

2.2 Elastic local buckling property of square hollow section joint panels

Fig. 4(a) shows the relationship between the shear buckling coefficient k_τ derived by the energy method and aspect ratio λ (= L/b) on the panel webs. The parameter is the gradients of bending moment β_c and β_b. The gradients of bending moment are defined in Fig. 2. Here, the shear buckling coefficient under pure shear is also shown. The shear buckling coefficient under pure shear is calculated by Eq. (15) with high accuracy [9].

$$k_\tau = 5.34 + \frac{4.00}{\lambda^2} \tag{15}$$

The results show that as the gradients of bending moment increase, the shear buckling coefficient increases. Additionally, when the gradients of bending moment exceed (β_c, β_b) = (1.0, 1.0), regardless of the aspect ratio, the shear buckling coefficients are larger than the shear buckling coefficient under pure shear. Fig. 4(b) shows the relationship between the shear buckling coefficient k_τ and aspect ratio λ (= L/b) on the panel flanges. The parameters are the gradients of bending moment β_c and β_b, and the restraint effect of H-shaped section beam webs on a centerline of the panel flanges. The results show that regardless of the restraint effect, as the gradients of bending moment increase, the shear buckling coefficient increases. Moreover, regardless of the gradients of bending moment, the shear buckling coefficient increases from 3 to 4 times with considering the restraint effect.

Fig. 5(a) shows the buckling mode of the panel web at the point A in Fig. 4(a). The contour lines in the Fig. 5(a) indicate the amount of deformation in the out-of-plain direction normalized by the maximum amount of deformation in the increments of 0.2. The mode indicates shear-type. Similarly, Fig. 5(b) shows the buckling mode of the panel flange at the point B in Fig. 4(b). The mode indicates bending-type at the end of the panel flange.

Fig. 6 shows the relationship between the shear buckling coefficient k_τ and aspect ratio λ (= L/b) on the panel webs. The parameter is the ratio of maximum bending stress $\sigma_{xcr}/\sigma_{ycr}$. The maximum bending stress σ_{xcr} in the x-axis direction and σ_{ycr} in the y-axis direction are defined in Fig. 2. The results show that regardless of the aspect ratio, the effect of the ratio of maximum bending stress on the shear buckling coefficient is small.

Fig. 7(a) shows the local buckling plate elements in the case of (β_c, β_b) = (1.0, 1.0). The vertical axis indicates the ratio of maximum bending stress $\sigma_{xcr}/\sigma_{ycr}$, and the horizontal axis indicates the normalized gradient of bending moment β/λ. The hollow circle ○ indicates that the web locally buckles earlier than the flange. The hollow square □ indicates that the flange locally buckles earlier than the web. In order to judge the local buckling plate elements, the shear buckling coefficients of the panel webs and flanges are compared. It is assumed that the buckling occurs on the plate elements which have the smaller shear buckling coefficient. From the figure, since all of the plots are □, the panel flanges locally buckle earlier than the panel webs in case of (β_c, β_b) = (1.0, 1.0). Similarly, Fig. 7(b) shows the local buckling plate element in the case of (β_c, β_b) = (2.0, 2.0). From the figure, since all of the plots are ○, the panel webs locally buckle earlier than the panel flanges.

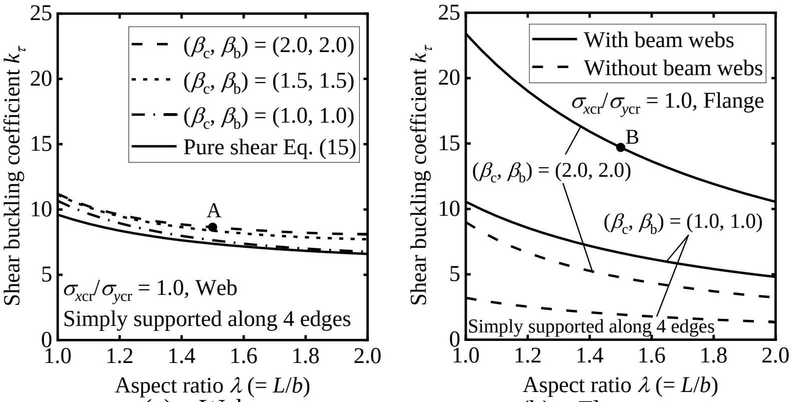

(a) Web (b) Flange

Fig. 4 Effect of gradients of bending moment

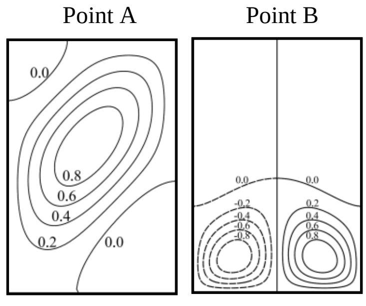

(a) Web (b) Flange

Fig. 5 Buckling mode

(β_c, β_b) = (2.0, 2.0)

$\sigma_{xcr}/\sigma_{ycr}$ = 1.0

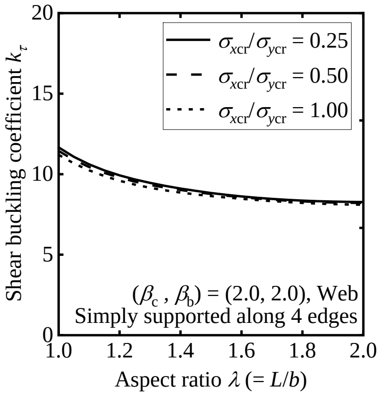

Fig. 6 Effect of ratio of maximum bending stress

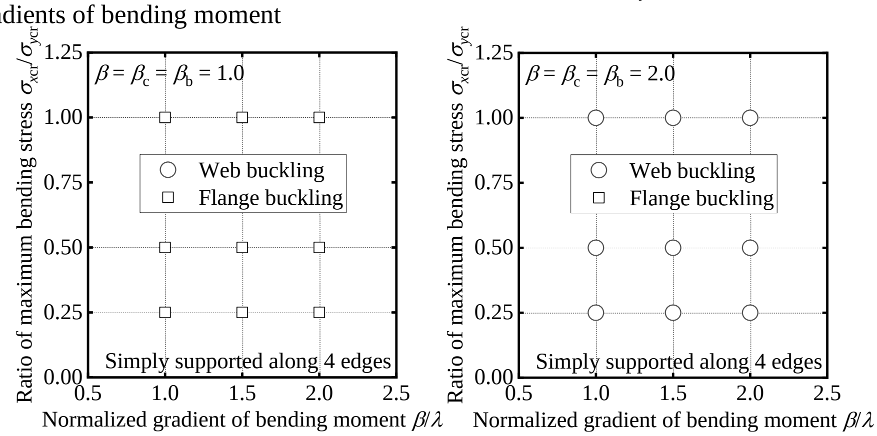

(a) (β_c, β_b) = (1.0, 1.0) (b) (β_c, β_b) = (2.0, 2.0)

Fig. 7 Buckling plate element

3 CYCLIC LOADING ANALYSIS OF SQUARE STEEL TUBE JOINT PANELS

In this chapter, large deformation behavior, ultimate strength, and plastic deformation capacity of square steel tube joint panels are investigated with the finite element method.

3.1 Overview of finite element method analysis

An elasto-plastic finite element analysis considering geometric nonlinearity was conducted using the general-purpose analysis program Abaqus. Fig. 8 shows the planar cross-shaped beam-column connection frame model. The boundary conditions at the ends of the beams and columns are also shown in the figure. The analysis models are composed of four-node shell elements, and rigid elements are introduced at the ends of the beams and columns to restrain warping. Loading is controlled by vertical displacement at the ends of the beams. Fig. 9 shows the cyclic loading hysteresis with increasing amplitude three cycles for each positive and negative direction. The vertical displacement δ at the ends of the beams of the amplitudes is 1, 2, 3, ..., and 10 times the vertical displacement δ_p at the ends of the beams with joint panel yielding. Table 1 shows the cross-sectional shapes of the members and mechanical property of steel. Both the joint panel and columns do not have corner radius, and the material property of the flat parts of cold-formed square steel tubes are applied to the joint panels and the columns. A combined hardening rule is used for the materials. Table 1 also shows the parameters of the considered analytical models. The parameters are the panel width–thickness ratio B/t, panel aspect ratio λ (= L/b), and length of beams L_b. In all models, the gradients of bending moment are fixed at (β_c, β_b) = (2.0, 2.0), and the length of columns L_c is 1500 mm. The definition of the gradients of bending moment are the same as that shown in Fig. 2 in Chapter 2.

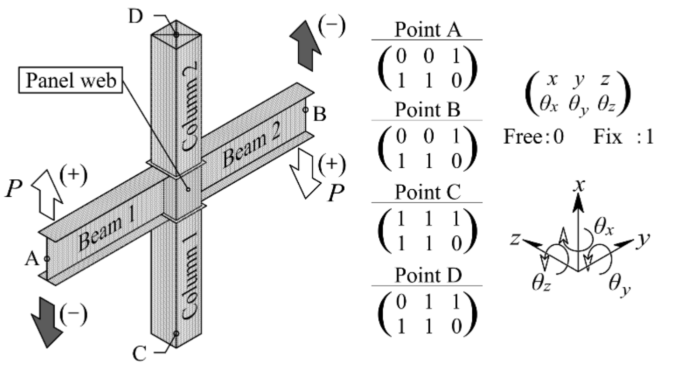

Fig. 8 Analysis model

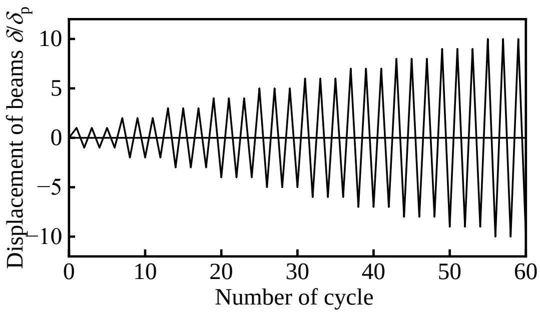

Fig. 9 Loading history

Table 1 Property of member and material

		Section size	Length [mm]	Material	Young's modulus E [N/mm²]	Yield strength σ_y [N/mm²]	Tensile strength σ_u [N/mm²]
Beam	Web	H-L×200×9×14	* Table 2	SN490	2.05×10^5	405	554
	Flange						
Column		□-303×303×12	1500	BCR295	1.98×10^5	334	484
Joint panel		□-(291+t)×(291+t)×t	* Table 2	BCR295	1.98×10^5	334	484
Diaphragm		PL-19×350×350	-	SN490	2.05×10^5	405	554

Table 2 Property of frame model

No.	Panel width–thickness ratio B/t [-]	Panel aspect ratio λ (= L/b) [-]	Length of beam L_b [mm]
1	19.2 (t = 16)	1.0	3000
2		1.5	
3	21.8 (t = 14)	1.0	
4		1.5	
5		2.0	
6	25.3 (t = 12)	1.0	
7		1.5	
8		2.0	
9	33.3 (t = 9)	1.0	
10		1.5	
11		2.0	
12	49.5 (t = 6)	1.0	
13		2.0	
14	33.3 (t = 9)	1.5	2000
15			4000

The panel shear force ${}_{\mathrm{p}}Q$ and shear strain γ are calculated using Eqs. (16) and (17) [3].

$$ {}_{\mathrm{p}}Q = \left(\frac{2L_{\mathrm{b}}}{L} - \frac{2L_{\mathrm{b}} + b}{2L_{\mathrm{c}} + L}\right) \cdot P \tag{16} $$

$$ \gamma = \frac{1}{2L\cos\theta}\{d_1 + d_2 - (v_{\mathrm{A}} - v_{\mathrm{B}})\sin\theta\} \tag{17} $$

Here, L_c is the length of columns (= 1500 mm), L_b is the length of beams, L is the length of joint panels, b is the center-to-center distance of the joint panel thickness, P is the vertical external force on ends of beams, θ is the angle of diagonals within panel webs, d_1 and d_2 are the diagonal displacements at corners of panel webs, and v_A and v_B are the vertical displacements at corners of panel webs. The panel yielding shear strength ${}_{\mathrm{p}}Q_{\mathrm{p}}$ and yielding shear strain γ_p are calculated by Eqs. (18) and (19). The yielding shear stress τ_y is calculated by Eq. (20).

$$ {}_{\mathrm{p}}Q_{\mathrm{p}} = 2bt\tau_{\mathrm{y}} \tag{18} $$

$$ \gamma_{\mathrm{p}} = \frac{2(1+\nu)\tau_{\mathrm{y}}}{E} \tag{19} $$

$$ \tau_{\mathrm{y}} = \frac{\sigma_{\mathrm{y}}}{\sqrt{3}} \tag{20} $$

Here, t is thickness of joint panels, ν is Poisson's ratio ($\nu = 0.3$), E is Young's modulus, and σ_y is yield stress.

3.2 Cyclic local buckling behavior of square steel tube joint panels

Fig. 10 shows the normalized load–displacement relationships of the models No. 3–5. The normalized panel shear force ${}_pQ/{}_pQ_p$ on the vertical axis is calculated by dividing the panel shear force ${}_pQ$ by the panel yielding shear strength ${}_pQ_p$. The normalized shear strain γ/γ_p on the horizontal axis is calculated by dividing the panel shear strain γ by the panel yielding shear strain γ_p. The solid triangle ▼ indicates the point of the positive-side ultimate strength, while the hollow triangle ▽ indicates the point of the negative-side ultimate strength. The results show that as the panel aspect ratio decreases, the load–displacement relationships in both positive and negative directions become more stable spindle-shaped hysteresis curves.

Fig. 11(a) shows the deformed configuration of the joint panel at the point of the ultimate strength for the model No. 4. For better visualization, the deformation is magnified by a factor of two. In many models, local buckling of the panel web is observed as shown in the figure. This phenomenon is the determining factor of the ultimate strength. On the other hand, Fig. 11(b) shows the deformed configuration of the columns at the point of the ultimate strength for the model No. 5. In the model No. 5, local buckling occurs in the column as shown in the figure. As a result, in Fig.11(c), there is almost no apparent strength degradation after reaching the ultimate strength of joint panels, and the response became biased toward the negative deformation side in the model No. 5. This behavior is due to the earlier occurrence of local buckling in the column rather than in the joint panel.

Fig. 12(a) shows the effect of the panel width–thickness ratio B/t on the normalized load–displacement relationship. The normalized load–displacement relationship is represented by the skeleton curves. The skeleton curves are created by tracing the peak points of each hysteresis loop from the load–displacement curves. The results show that as the panel width–thickness ratio increases, the ultimate strength and the deformation at the point of the ultimate strength decrease. Similarly, Fig. 12(b) shows the effect of the panel aspect ratio λ ($= L/b$) on the load–displacement relationship. The results show that as the panel aspect ratio increases, the ultimate strength decreases. Fig. 12(c) shows the effect of length of beams L_b on the load–displacement relationship. From the figure, the effect of the length of beams is almost not observed.

Fig. 13(a) shows the relationship between the panel width–thickness ratio B/t and either the rate of increase of the ultimate strength ${}_pQ_{max}/{}_pQ_p$ or the plastic deformation rate γ_{max}/γ_p-1 at the point of the ultimate strength. The rate of increase of the ultimate strength of the left vertical axis is calculated by dividing the panel ultimate strength ${}_pQ_{max}$ by the panel yielding shear strength ${}_pQ_p$. The plastic deformation capacity of the right vertical axis is calculated by dividing the panel shear strain γ_{max} at the point of ultimate strength on the skeleton curve by the panel yielding shear strain γ_p. Here, the result for the model No. 5 is excluded due to the buckling in the columns. The results show that as the panel width–thickness ratio increases, both the rate of increase of the ultimate strength and the plastic deformation capacity at the point of the ultimate strength tend to decrease. Similarly, Fig. 13(b) shows the relationship between the panel aspect ratio λ ($= L/b$) and either the rate of increase of the ultimate strength ${}_pQ_{max}/{}_pQ_p$ or the plastic deformation rate γ_{max}/γ_p-1. The results show that as the panel aspect ratio increases, both the rate of increase of the ultimate strength and the plastic deformation capacity tend to decrease. It should be noted that the trend observed for the panel aspect ratio in elsto-plastic local buckling behavior is consistent with the trend of the elastic local buckling coefficient discussed in Chapter 2.

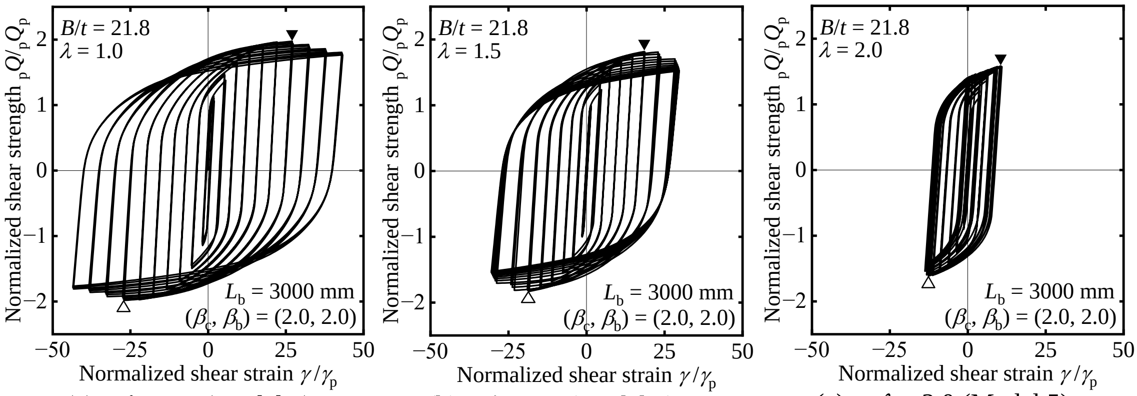

(a) λ = 1.0 (Model 3) (b) λ = 1.5 (Model 4) (c) λ = 2.0 (Model 5)

Fig. 10 Load–displacement curve
(B/t = 21.8, L_b = 3000 mm, (β_c, β_b) = (2.0, 2.0))

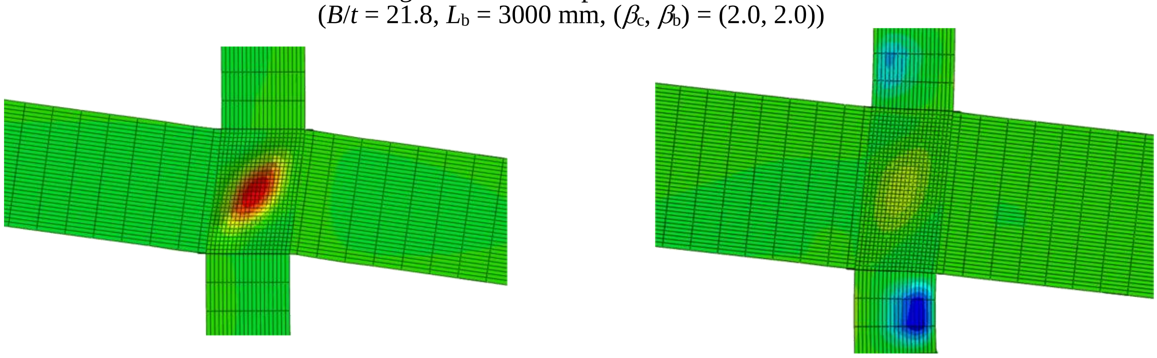

(a) Local buckling on joint panel (Model 4) (b) Local buckling on column (Model 5)

Fig. 11 Deformed configuration of connection at ultimate strength
(B/t = 21.8, L_b = 3000 mm, (β_c, β_b) = (2.0, 2.0))

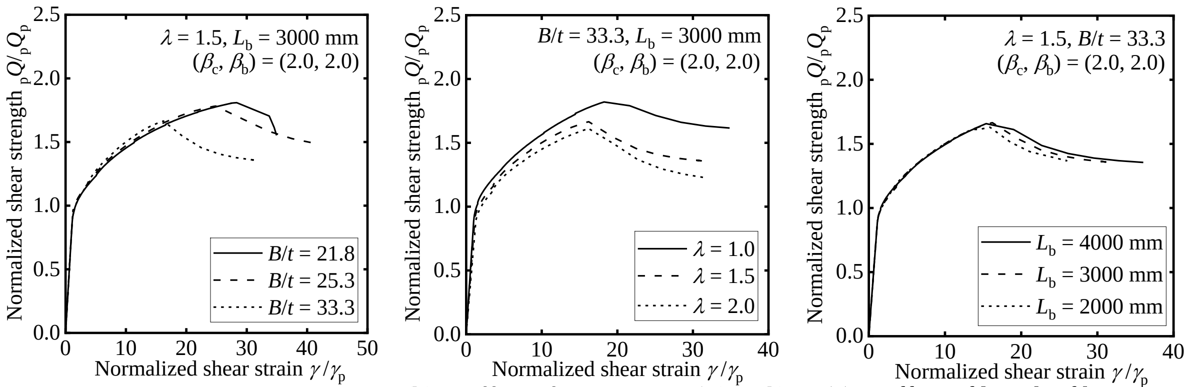

(a) Effect of panel width–thickness ratio B/t (Model 4, 7, and 10) (b) Effect of aspect ratio λ (= L/b) (Model 9~11) (c) Effect of length of beams L_b (Model 10, 14, and 15)

Fig. 12 Effect of member shapes ((β_c, β_b) = (2.0, 2.0))

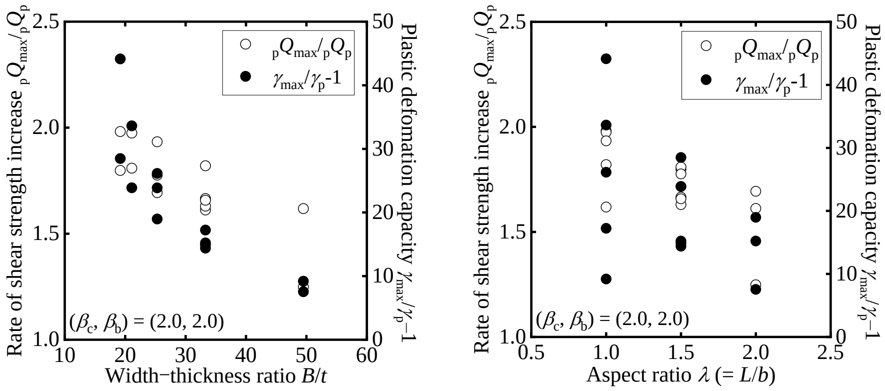

(a) Effect of panel width–thickness ratio B/t (b) Effect of panel aspect ratio λ (= L/b)

Fig. 13 Relationship between ${}_pQ_{max}/{}_pQ_p$ or γ_{max}/γ_p−1 and member shapes ((β_c, β_b) = (2.0, 2.0))

4 EVALUATION OF SEISMIC PERFORMANCE OF SQUARE STEEL TUBE JOINT PANELS

Fig. 14(a) shows the relationship between the normalized width–thickness ratio $({}_{p}Q_{p}/{}_{p}Q_{cr})^{1/2}$ and the rate of increase of the ultimate strength ${}_{p}Q_{max}/{}_{p}Q_{p}$. The panel shear buckling strength ${}_{p}Q_{cr}$ used for the normalized width–thickness ratio in the horizontal axis is calculated using the shear buckling coefficient derived in Chapter 2. The plots follow Table 3. Here, the result for the model No. 5 is excluded since the model locally buckles earlier in the column. The results show that as the normalized width–thickness ratio increases, the rate of increase of the ultimate strength tends to decrease. Fig. 14(b) shows the relationship between the normalized width–thickness ratio $({}_{p}Q_{p}/{}_{p}Q_{cr})^{1/2}$ and the plastic deformation rate $\gamma_{max}/\gamma_{p}-1$ at the point of the ultimate strength. The results show that as the normalized width–thickness ratio increases, the plastic deformation capacity tends to decrease. Therefore, it can be considered that reasonable evaluation of the ultimate strength and plastic deformation capacity based on the normalized width–thickness ratio is possible.

Fig. 15 shows the relationship between the cumulative plastic deformation rate $\Sigma\gamma_{max}/\gamma_{p}-1$ and plastic deformation rate $\gamma_{max}/\gamma_{p}-1$ at the point of the ultimate strength. The normalized load-deformation relationship is constructed using the cumulative curve by connecting each half-cycle of the hysteresis curves in the positive loading direction. The normalized shear strain at the point of ultimate strength on the cumulative curve is defined as the cumulative plastic deformation capacity. From the figure, the cumulative plastic deformation capacity and plastic deformation capacity are almost linearly related as expressed by Eq. (21).

$$\Sigma\gamma_{max}/\gamma_{p} - 1 = 3.50 \cdot (\gamma_{max}/\gamma_{p} - 1) \tag{21}$$

Table 3 Plot in figures

No.	Plot	No.	Plot	No.	Plot	No.	Plot
1	□	5		9	■	13	◀
2	○	6	◁	10	●	14	▶
3	▽	7	▷	11	▼	15	★
4	△	8	☆	12	▲		

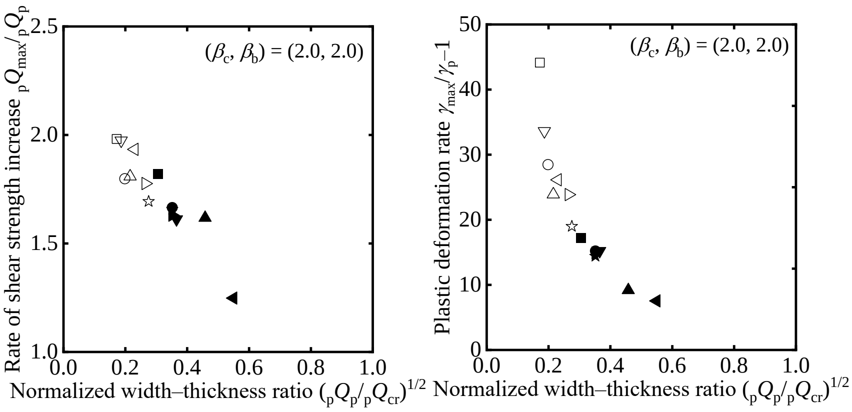

(a) ${}_{p}Q_{max}/{}_{p}Q_{p}$ (b) $\gamma_{max}/\gamma_{p}-1$

Fig. 14 Relationship between ${}_{p}Q_{max}/{}_{p}Q_{p}$ or $\gamma_{max}/\gamma_{p}-1$ and $({}_{p}Q_{p}/{}_{p}Q_{cr})^{1/2}$ $((\beta_c, \beta_b) = (2.0, 2.0))$

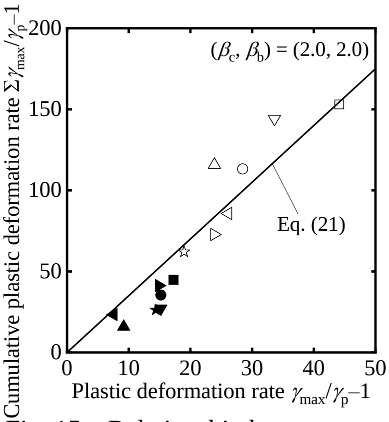

Fig. 15 Relationship between $\Sigma\gamma_{max}/\gamma_{p}$-1 and $\gamma_{max}/\gamma_{p}-1$ $((\beta_c, \beta_b) = (2.0, 2.0))$

5 CONCLUSION

The buckling eigenvalue analysis was conducted using the energy method for the joint panel in the planar cross-shaped connection frame composed of square steel tube columns and H-shaped steel beams to derive the elastic local buckling strength. Additionally, the finite element analysis was also conducted to investigate the ultimate strength and plastic deformation capacity of the joint panels. The obtained findings are presented below.

- As the gradients of bending moment β_c, β_b increases, the shear buckling coefficient k_τ increases, and the shear-type buckling mode on the panel webs becomes more pronounced.
- The ratio of maximum bending stress $\sigma_{xcr}/\sigma_{ycr}$ has little effect on the shear buckling coefficient k_τ.
- Considering the restraint effect of H-shaped beam webs on the panel flanges, the shear buckling coefficient k_τ becomes from 3 times to 4 times as much as without the restraint.
- It was confirmed that as the panel width–thickness ratio B/t increases, the ultimate strength ${}_pQ_{max}/{}_pQ_p$ and plastic deformation rate γ_{max}/γ_p-1 at the point of the ultimate strength decrease. Additionally, it was also confirmed that as the panel aspect ratio λ increases, the ultimate strength ${}_pQ_{max}/{}_pQ_p$ decreases.
- The effect of the length of beams L_b on the ultimate strength and plastic deformation capacity is small. Comparing the ultimate strength in the case of L_b = 2000 and 4000 mm, the difference of the ultimate strength is 0.01%.
- It was shown that the ultimate strength ${}_pQ_{max}/{}_pQ_p$ and plastic deformation rate γ_{max}/γ_p-1 can be reasonably evaluated using normalized width–thickness ratio $({}_pQ_p/{}_pQ_{cr})^{1/2}$.
- An approximately linear relationship between the cumulative plastic deformation capacity $\Sigma\gamma_{max}/\gamma_p-1$ and plastic deformation capacity γ_{max}/γ_p-1 is observed. The cumulative plastic deformation capacity is about 3.5 times the plastic deformation capacity in the range investigated in this study.

REFERENCES

[1] Hisashi N., Mototsugu T. and Tsuyoshi T., "Evaluation for Full Plastic Strength of Joint Panels in Hollow Section Column to Beam Connections", *Steel Construction Engineering, JSSC,* Vol. 11, No. 42, pp. 15–28, 2004

[2] Kikuo I., Yuichi U. and Kazuya M., "Elastic Shear Buckling Strength of L-Shaped Beam-to-Column Joint Panels Composed with I-Shaped Members", *Journal of Structural and Construction Engineering, AIJ,* Vol. 85, No. 77, pp. 759–769, 2020

[3] Susumu K. and Kazuo I., "The Shear Force Loading Test for the Beam-to-Column Joint Panels of Rectangular and Circular Hollow Section", *Journal of Structural and Construction Engineering, AIJ,* No. 502, pp. 149–156, 1997

[4] Takehito K., Susumu K. and Ichiro I., "The Test for Cruciform Sub Assemblages of the Joint Panels at the Connection of Rectangular Steel Column to H-Shaped Beam, Varied Width–thickness Ratio of the Joint Panels", *Proceedings of Architectural Meetings, Kanto Chapter, AIJ,* pp. 309–312, 1998

[5] Ben M., Xi L., Yongtao B. and Lisa W., "Shear Behavior of Panel Zones in Steel Beam-to-Column Connections with Unequal Depth of Outer Annular Stiffener", *Journal of Structural Engineering*, No. 145, 04018247, 2019

[6] Jun H., Teruhiko Y., Hideaki T., Yuqing L., Airong C. and Masashi I., "Experimental and Numerical Study on the Behavior of Steel Beam-to-Column Connections under Cyclic Loading", *International Journal of Steel Structure*, Vol. 10, No. 2, pp. 131–146, 2010

[7] Qi L., Zuhong T., Cuihong W., Hua J. and Enhe B., "Plastic Damage Distribution of Beam–Column Joint Consisting of H-Shaped Steel", *Engineering and Computational Mechanics*, Vol. 175, No. 1, pp. 29–37, 2022

[8] Timoshenko S. P. and Gere J. M., *Theory of Elastic Stability, McGraw-Hill Book Company*, 1961

[9] Theodore V. G., *Guide to Stability Design Criteria for Metal Structures*, 1998